

Two-Point Incremental Forming with Partial Die: Theory and Experimentation

M.B. Silva and P.A.F. Martins

(Submitted April 15, 2012; in revised form September 12, 2012; published online October 2, 2012)

This paper proposes a new level of understanding of two-point incremental forming (TPIF) with partial die by means of a combined theoretical and experimental investigation. The theoretical developments include an innovative extension of the analytical model for rotational symmetric single point incremental forming (SPIF), originally developed by the authors, to address the influence of the major operating parameters of TPIF and to successfully explain the differences in formability between SPIF and TPIF. The experimental work comprised the mechanical characterization of the material and the determination of its formability limits at necking and fracture by means of circle grid analysis and benchmark incremental sheet forming tests. Results show the adequacy of the proposed analytical model to handle the deformation mechanics of SPIF and TPIF with partial die and demonstrate that neck formation is suppressed in TPIF, so that traditional forming limit curves are inapplicable to describe failure and must be replaced by fracture forming limits derived from ductile damage mechanics. The overall geometric accuracy of sheet metal parts produced by TPIF with partial die is found to be better than that of parts fabricated by SPIF due to smaller elastic recovery upon unloading.

Keywords analytical model, circle grid analysis, formability, geometric accuracy, two-point incremental forming

1. Introduction

Conventional sheet metal forming is a highly competitive industrial activity characterized by low profit margins that are primarily due to high capital investment in presses, auxiliary equipment, and dedicated tool systems. Industrial applications, running on either compounded tools in which parts are produced in one press stroke or in progressive tools that carry the blanks from one station to the next until the desired shape is obtained, determine that conventional sheet metal forming is only economically feasible for mass production (large batch sizes).

To succeed in the face of global competition, sheet metal forming companies are trying to extend their portfolio of applications to small-batch size and customized value added products and services. Because new business requires the utilization of agile and flexible sheet metal forming processes that are capable of reducing the operative costs of fabrication to a level where small-batch production becomes economically feasible, attention is being focused towards 'incremental sheet forming' (ISF) processes.

The key advantage of ISF over conventional sheet metal forming is that presses and dedicated tool systems are replaced by simple, low-cost, forming tools with hemispherical tips that move over custom-designed numerically controlled tool paths in order to shape sheets into parts by progression of localized deformation.

Single point incremental forming (SPIF) has been the most widely utilized and investigated type of ISF process. The state-of-the-art, potential applications and fundamentals of SPIF are comprehensively described in Jeswiet et al. (Ref 1), Jackson and Allwood (Ref 2), and Martins et al. (Ref 3) and the basic components of the process are schematically shown in Fig. 1(a): (i) the blank, (ii) the blank holder, (iii) the rig with the backing plate (beneath the blank), and (iv) the forming tool.

On contrary to SPIF, where there is no backup die supporting the back surface of the sheet, there is a variant of ISF named 'two-point incremental forming' (TPIF) in which the blank is formed against a partial or a full die. As shown in Fig. 1(b), in TPIF the sheet is rigidly clamped around its periphery with a blankholder that moves vertically and the forming tool moves along a trajectory on the outer surface of the sheet part, from the top to the bottom of the geometry.

Partial dies only support essential areas of the blank (Fig. 1b) and its geometry can be arbitrary in order to allow producing different but similar shapes. Full dies support the entire blank and, therefore, offer the advantage of controlling deformation and improving accuracy through physical constraint of the sheet. However, full dies are much less flexible than partial dies because like in conventional sheet metal forming, each full die is dedicated to a specific part to be fabricated.

Contrary to SPIF, most of the published research in TPIF over the past years has been mainly concerned with applications and formability limits of the process. Matsubara (Ref 4) investigated different tool paths for producing cones and pyramids with an arbitrary number of sides and concluded that TPIF with partial die allows producing a wide range of complex three-dimensional shapes. Matsubara also claimed that the wall thickness of TPIF parts follow the sine law of shear spinning. Attanasio et al. (Ref 5) investigated tool path optimization strategies with the objective of improving the overall surface quality and geometric accuracy of an automotive component

M.B. Silva and P.A.F. Martins, IDMEC, Instituto Superior Técnico, Technical University of Lisbon, Av. Rovisco Pais, 1049-001 Lisbon, Portugal. Contact e-mail: pmartins@ist.utl.pt.

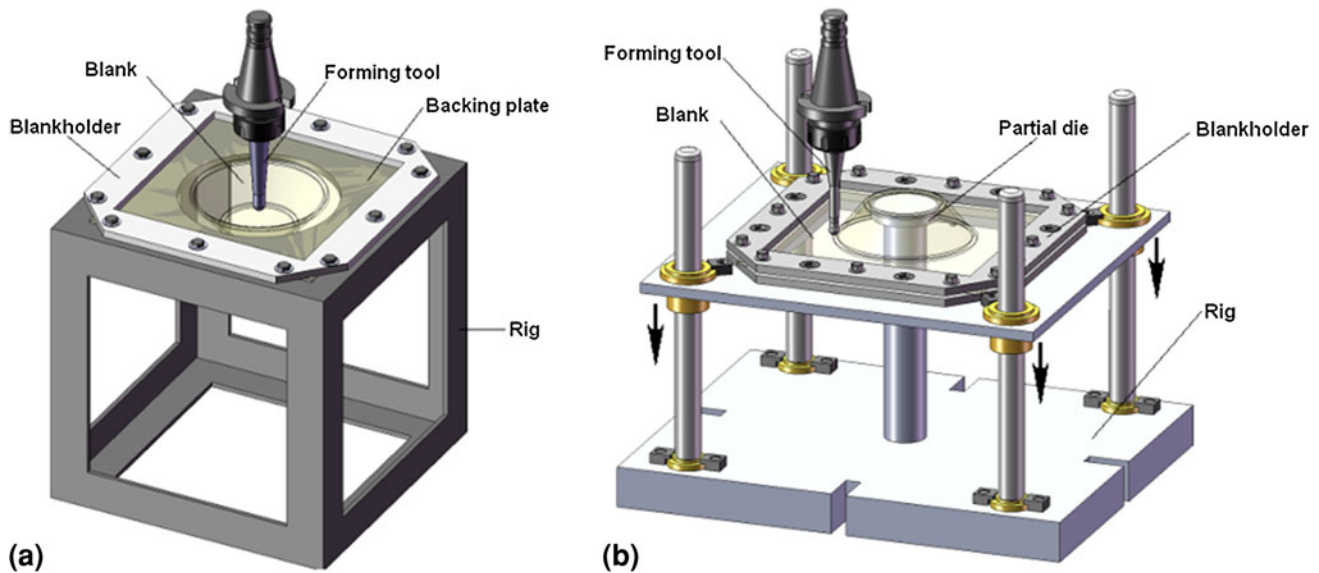


Fig. 1 Schematic representation of the experimental setup for incremental sheet forming process variants. (a) Single point incremental forming (SPIF). (b) Two-point incremental forming (TPIF)

produced by TPIF. Jeswiet et al. (Ref 6) determined the magnitude of the forces and Hirt et al. (Ref 7) compared the forces and the geometrical accuracy in pyramidal benchmark parts produced by TPIF with partial and full dies. Hirt et al. (Ref 7) also reported the utilization of metallic foams to produce self-configuring full dies as an alternative to rigid dies.

The state-of-the-art in TPIF is comprehensively described in Jeswiet et al. (Ref 1) and despite the above-mentioned research efforts and fundamental research work performed by Jackson and Allwood (Ref 2), there is still a need to examine the deformation mechanics, to describe the physics behind failure and to understand the differences and similarities between SPIF and TPIF with partial die.

This paper is focused on the aforementioned subjects and is aimed to provide answers to the following key questions: What is the distribution of the strain and stress during plastic deformation in the small contact region between the tool and the sheet? What is the failure mechanism? Is it possible to develop a unified analytical model that can easily explain the differences in formability between SPIF and TPIF with partial die?

In what regards theoretical developments, the aim of the present paper is to extend the previous analytical model based on the enhanced membrane analysis for rotational symmetric SPIF that was developed by Silva et al. (Ref 8) into a unified theoretical framework, founded on the physics of the processes, which can easily handle SPIF and TPIF with partial die. Experimental work consisting of circle grid analysis, mechanical and formability characterization of the material, and fabrication of benchmark sheet metal parts, gives support to the theoretical developments. The overall investigation provides a new level of insight of TPIF with partial die.

2. Theoretical Background

Circle grid analysis in conjunction with experimental observations of the smear-marks in the small contact region between the tool and the sheet allowed authors to conclude that

rotational symmetric SPIF and TPIF with partial die are performed under plane strain conditions. The state of stress in the region can be derived from the enhanced membrane analysis for rotational symmetric conditions assuming material to be isotropic and rigid-perfectly plastic, bending moments to be neglected and circumferential, meridional and thickness directions to be principal directions.

2.1 State of Stress and Strain

Figure 2(a) presents a schematic representation of incremental forming tool acting on a sheet during rotational symmetric SPIF or TPIF with partial die. The material is stretched under plane strain conditions so that it conforms to the hemispherical shape of the tool, forming a local plastic deformation region (CDEF) in the sheet.

Resolving force equilibrium in the thickness, circumferential and meridional directions that are shown in Fig. 2(b), under the abovementioned simplifying assumptions, and taking into consideration that friction stress exerted at the tool-sheet contact interface is made of a meridional component $-\mu_\phi \sigma_t$ and a circumferential component $-\mu_\theta \sigma_r$, the equilibrium conditions under bi-directional contact friction forces are:

$$\begin{aligned} & \sigma_t r d\theta r_1 d\alpha + \sigma_\phi r d\theta t \sin \frac{d\alpha}{2} \\ & + (\sigma_\phi + d\sigma_\phi) (r + dr) d\theta (t + dt) \sin \frac{d\alpha}{2} \\ & + \sigma_\theta r_1 d\alpha t \sin \frac{d\theta}{2} \cos \alpha + (\sigma_\theta + d\sigma_\theta) r_1 d\alpha t \sin \frac{d\theta}{2} \cos \alpha = 0 \end{aligned} \quad (\text{Eq 1})$$

$$\begin{aligned} & \sigma_\theta r_1 d\alpha \left(t + \frac{dt}{2} \right) - \mu_\theta \sigma_t r_1 d\alpha \left(r + \frac{dr}{2} \right) d\theta \\ & - (\sigma_\theta + d\sigma_\theta) r_1 d\alpha \left(t + \frac{dt}{2} \right) = 0 \end{aligned} \quad (\text{Eq 2})$$

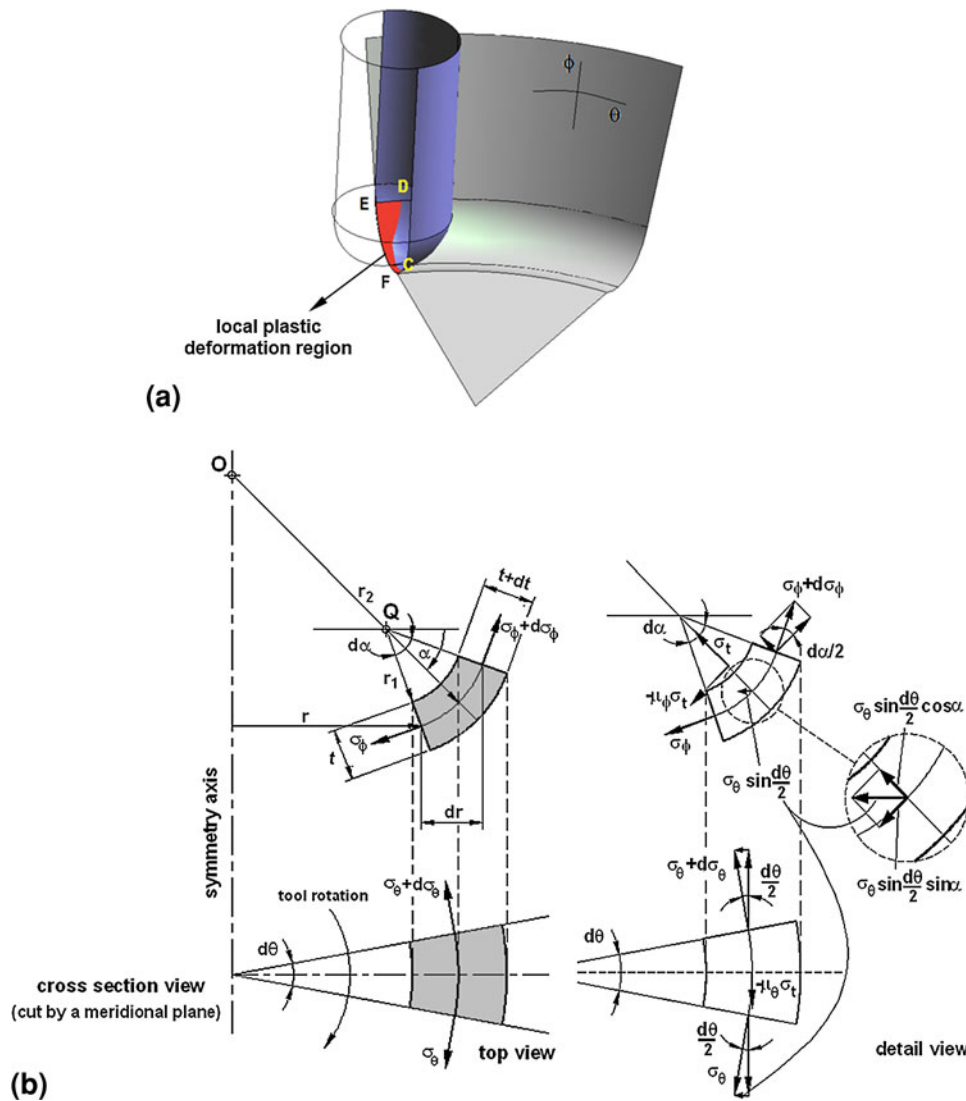


Fig. 2 Essentials for the theoretical framework. (a) Schematic representation of the contact area (local plastic deformation region, CDEF) between the tool and sheet. (b) Cross section view showing the stresses applied in meridional, circumferential, and thickness directions to the local plastic deformation region (CDEF)

$$\begin{aligned}
 & (\sigma_\phi + d\sigma_\phi) (r + dr) d\theta (t + dt) - \sigma_\phi r d\theta t \\
 & + \mu_\phi \sigma_t r d\theta r_1 d\alpha - \sigma_\theta \frac{d\theta}{2} r_1 d\alpha t \sin \alpha \\
 & - (\sigma_\theta + d\sigma_\theta) \frac{d\theta}{2} r_1 d\alpha t \sin \alpha = 0 \quad (\text{Eq 3})
 \end{aligned}$$

In case of SPIF, the distribution of stress in the local plastic deformation region CDEF is derived from Eq (1)-(3) after neglecting higher order terms, taking into account geometrical simplifications and considering the Tresca yield criterion. Table 1 resumes the strains and stresses in rotational symmetric SPIF that were obtained from the equilibrium equations under plane strain conditions. Details can be found in Silva et al. (Ref 8).

The first step to develop a unified theoretical framework that can easily handle the modes of deformation that are commonly found in rotational symmetric SPIF and TPIF with partial die consists in assuming the superposition principle and the meridional stresses to be additive. In

practical terms, the resultant meridional stress σ_ϕ in TPIF with partial die is made equal to the sum of individual contributions due to equilibrium in the local plastic deformation region located at the transition between the inclined wall and the corner radius of the sheet $\sigma_\phi^{\text{spif}}$ and to external loading applied by the blank holder σ_ϕ^{bh} during its vertical movement. The first contribution is local and identical to that of conventional SPIF while the second is exclusive of TPIF with partial die and gives rise to a uniform distribution of meridional stresses (Fig. 3),

$$\sigma_\phi = \sigma_\phi^{\text{spif}} + \sigma_\phi^{\text{bh}} \quad (\text{Eq 4})$$

where,

$$\sigma_\phi^{\text{bh}} = \frac{F_{\text{bh}}}{2\pi r t \sin \psi} = \frac{m_{\text{bh}} g}{2\pi r t \sin \psi} \quad (\text{Eq 5})$$

The symbol m_{bh} denotes the blank holder mass, g is the acceleration of gravity, and ψ is the draw angle between the inclined wall and the initial flat configuration of the sheet.

Table 1 State of stress and strain in rotational symmetric SPIF and TPIF

	Assumption	State of strain	State of stress	Hydrostatic stress
SPIF	Plane strain conditions	$d\varepsilon_\phi = -d\varepsilon_t > 0$ $d\varepsilon_\theta = 0$ $d\varepsilon_r < 0$	$\sigma_\phi = \sigma_1 = \frac{\sigma_Y r_{\text{tool}}}{r_{\text{tool}} + t} > 0$ $\sigma_\theta = \sigma_2 = \frac{1}{2}(\sigma_1 + \sigma_3)$ $\sigma_t = \sigma_3 = -\frac{\sigma_Y t}{r_{\text{tool}} + t} < 0$	$\sigma_m = \frac{\sigma_Y (r_{\text{tool}} - t)}{2(r_{\text{tool}} + t)}$
TPIF	Plane strain conditions	$d\varepsilon_\phi = -d\varepsilon_t > 0$ $d\varepsilon_\theta = 0$ $d\varepsilon_r < 0$	$\sigma_\phi = \sigma_1 = \frac{\sigma_Y r_{\text{tool}} - \sigma_\phi^{\text{bh}} t}{r_{\text{tool}} + t} > 0$ $\sigma_\theta = \sigma_2 = \frac{1}{2}(\sigma_1 + \sigma_3)$ $\sigma_t = \sigma_3 = -\frac{(\sigma_Y + \sigma_\phi^{\text{bh}}) t}{r_{\text{tool}} + t} < 0$	$\sigma_m = \frac{\sigma_Y (r_{\text{tool}} - t) - 2 \sigma_\phi^{\text{bh}} t}{2(r_{\text{tool}} + t)}$

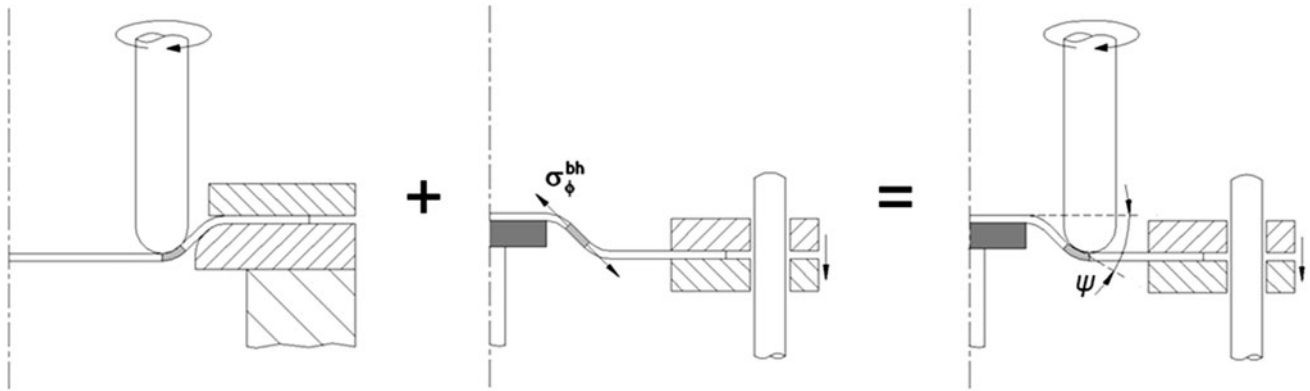


Fig. 3 Schematic representation of the superposition principle that was utilized to determine the stress field in TPIF with partial dies

Table 1 presents the state of stress in rotational symmetric TPIF with partial die that was obtained after combining the equilibrium Eq (1)-(3) and the uniform distribution of meridional stresses due to the blank holder (Ref 5) under the superposition principle. In case $\sigma_\phi^{\text{bh}} = 0$ the well-known state of stress of SPIF results.

2.2 Hydrostatic Stress

The onset of failure by fracture occurs when a damage function D that usually takes the form,

$$D = \int_0^{\bar{\varepsilon}_f} f\left(\frac{\sigma_m}{\sigma_Y}\right) d\bar{\varepsilon} \tag{Eq 6}$$

reaches a critical value D_c , where $\bar{\varepsilon}_f$ denotes the effective true strain at failure (Ref 9).

The triaxiality ratio σ_m/σ_Y plays an important role in the characterization of the formability limits by means of ductile damage mechanics and, therefore, understanding the differences in formability between SPIF and TPIF with partial die requires comparing σ_m/σ_Y from the states of stress that are included in Table 1. Under these circumstances, by resorting to continuum rigid-plasticity, ignoring the presence of micro voids and assuming proportional loading, it can be claimed that the uniformly distributed meridional stress σ_ϕ^{bh} due to the blank holder is beneficial for lowering the triaxiality ratio σ_m/σ_Y of TPIF with partial dies,

$$\frac{\left(\frac{\sigma_m}{\sigma_Y}\right)_{\text{TPIF}}}{\left(\frac{\sigma_m}{\sigma_Y}\right)_{\text{SPIF}}} = \frac{\frac{(r_{\text{tool}} - t) - 2 \frac{\sigma_\phi^{\text{bh}} t}{\sigma_Y}}{2(r_{\text{tool}} + t)}}{\frac{(r_{\text{tool}} - t)}{2(r_{\text{tool}} + t)}} = 1 - 2 \frac{\sigma_\phi^{\text{bh}} t}{\sigma_Y (r_{\text{tool}} - t)} \cong 1 - \frac{\sigma_\phi^{\text{bh}}}{\sigma_Y} \tag{Eq 7}$$

This result leads to the conclusion that the rate of accumulated damage (Ref 6) in SPIF grows faster than in TPIF with partial die and explains the reason why the forming limits of TPIF with partial die are higher than those of SPIF. As a result of (Ref 7), it is worth mentioning that the influence of the radius of the tool r_{tool} is opposed to that of the thickness t of the sheet and to that of the mass m_{bh} of the blank holder. The formability in TPIF with partial die is expected to be higher than in SPIF when the radius of the tool r_{tool} decreases.

As will be comprehensively review and analysed in the fore coming sections of the paper, qualitative predictions based on the proposed unified theoretical framework are plausible and in good agreement with experimentation.

3. Experimentation

This section starts by describing the techniques that were utilized for performing the mechanical characterization and the independent determination of the formability limits of the material by necking and fracture and follows by presenting the experimental work plan that was designed for investigating the

differences and similarities in the mechanics of deformation of SPIF and TPIF with partial die.

3.1 Mechanical Characterization

The specimens utilized in the investigation were made from Aluminum AA1050-H111 sheet blanks with 1 mm thickness. The mechanical characterization of the material was performed by means of tensile tests in a universal materials testing machine (Instron 4507). The specimens were cut from the supplied sheet at 0°, 45°, and 90° with respect to the rolling direction in accordance with the ASTM Standard E8/E8M (Ref 10). The average stress-strain curve derived from the tensile tests is given by

$$\bar{\sigma} = 140 \bar{\epsilon}^{0.04} \text{ MPa.} \quad (\text{Eq 8})$$

The average values obtained for the yield stress σ_Y , the ultimate tensile strength σ_{UTS} , the modulus of elasticity E , and the elongation at break A are included in Table 2.

3.2 Formability Limits

The formability limits at necking (forming limit curve, FLC) and fracture (fracture forming limit line, FFL) were determined by combining the results from tensile tests with hydraulic bulge tests performed in a universal sheet testing machine (Erichsen 145/60) using bi-axial, circular (100 mm), and elliptical (100/63 mm) tooling sets. The technique utilized for obtaining the FLC involved electrochemical etching of a grid of overlapping circles with 2 mm initial diameter on the surface of the specimens before forming. Measurements of the major and minor axis of the ellipses that resulted from the plastic deformation of the circles during the formability tests allowed calculating the in-plane surface strains directly from (refer to the detail in Fig. 4)

$$\epsilon_1 = \ln \left(\frac{a}{2R} \right), \quad \epsilon_2 = \ln \left(\frac{b}{2R} \right), \quad (\text{Eq 9})$$

where the symbol R represents the original radius of the circle and the symbols a and b denote the major and minor axis of the ellipse.

The resulting FLC is plotted in Fig. 4 (refer to the gray curve) and was constructed by taking the principal strains (ϵ_1, ϵ_2) at failure from grid points placed just outside the neck (that is, adjacent to the region of intense localization) since they represent the condition of the uniformly thinned sheet just before necking occurs.

The technique utilized for obtaining the experimental FFL required measuring thickness before and after fracture in a microscope, at several places along the crack, in order to obtain the 'gauge length' strains (ϵ_1, ϵ_2). The strain in the width direction was obtained differently for tensile and bulge tests. In case of tensile tests measurements were directly taken from the

Table 2 Results from the tensile tests of Aluminum AA1050-H111

Parameter	Value
σ_Y , MPa	120
σ_{UTS} , MPa	121
A , %	10
E , MPa	70,943

width of the specimens whereas in case of bulge tests measurements made use of the imprinted grid of circles in order to obtain the initial and deformed reference lengths. Details of the technique can be found elsewhere (Ref 11).

The FFL was approximated by a black straight line $\epsilon_1 + 0.79 \epsilon_2 = 1.37$ falling from left to right and is bounded by a gray area corresponding to an error interval of 10% due to anisotropy and to experimental uncertainty in the determination of the strains at fracture. The large distance between the FLC and the FFL is responsible for the high level of formability attained in incremental forming of Aluminum AA1050-H111 sheets. This will be addressed later in this presentation.

As seen in Fig. 4, at the onset of local instability implying transition from the FLC representing necking towards the FFL, a sharp bend occurs in the strain path when testing is done with conventional bulge tests. The strain paths of bi-axial, circular, and elliptical bulge tests show a kink after neck initiation towards vertical direction, corresponding to plane strain conditions, as it is schematically plotted by the gray-dashed line for the circular bulge test. The strain paths of tensile formability tests also undergo a significant change of strain ratio from slope -2 to a steeper one, although not to vertical direction. The absence of a sharp kink of the strain path into vertical direction in tensile formability tests is due to the fact that major and minor strains after the onset of necking do not coincide with the original pulling direction. A comprehensive analysis on the direction of the strain paths in the tension-compression strain quadrant can be found in the work of Atkins (Ref 9, 12).

3.3 Experimental Work Plan in SPIF and TPIF

The experiments in SPIF and TPIF with partial die were performed in a Deckel Maho CNC machining center equipped with the rigs that are schematically shown in Fig. 1. The tests made use of square sheet blanks of Aluminum AA1050-H111 with dimensions of $250 \times 250 \times 1$ mm that were cut from the supplied sheets and the forming tools utilized in the experiments were made from cold working tool steel (120WV4-DIN, hardened and tempered to 60 HRC). The tools had hemispherical tips of 4 and 6 mm radius, their rotation was free and their

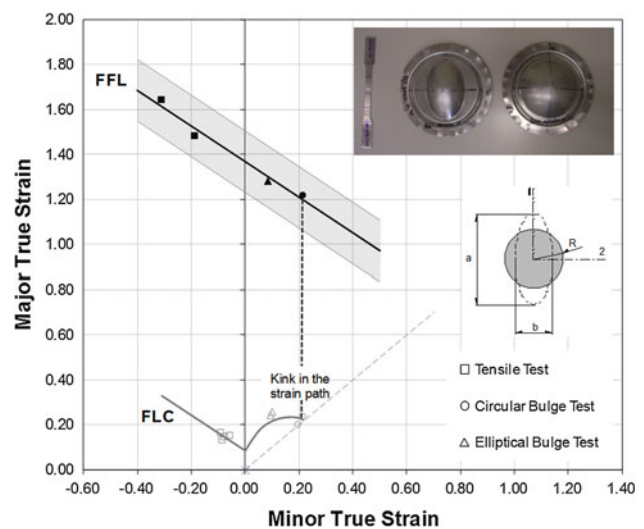


Fig. 4 Forming limit curve (FLC) and fracture forming limit line (FFL) for commercial sheets of Aluminum AA1050-H111 with 1 mm thickness in the principal strain space

feed rate was set to 1000 mm/min, corresponding to approximately 20% of the maximum feed rate of the CNC machining center. The tool path was circumferential with a step size per revolution equal to 0.2 mm and was generated with the commercial software MasterCAM. The lubricant applied between the forming tool and the sheet blank was the forming fluid Castrol Iloform TDN81.

The work plan included in Table 3 was designed in order to characterize the formability limits, to obtain the maximum drawing angle ψ_{\max} at fracture and to isolate the influence of the radius of the forming tool r_{tool} in TPIF with partial die. The experiments in SPIF were taken as reference test cases for comparison purposes.

The tests were performed in truncated conical shapes with progressively increasing and constant drawing angles $\psi(h)$ with the depth. The tests performed with progressively increasing drawing angles were based on a circular generatrix with a radius of 69.3 mm and provided a rough estimate of ψ_{\max} at fracture, which was subsequently fine-tuned by means of supplementary tests performed with constant drawing angles. The initial drawing angle of the tests that were performed with progressively increasing drawing angles was set to $\psi_{\max} = 30^\circ$.

By keeping the rest of the parameters at constant value, namely, (i) the thickness t of the sheet blanks, (ii) the tool path design, and (iii) the step size, feed rate, and rotation condition of the forming tool, because they had already been dealt with in previous investigations (Ref 1, 13), it was possible to reduce the total number of parameters that influence the process. Otherwise, the total number of possible combinations of variables to investigate would become quite large.

The formability limits were analysed by plotting the strain paths resulting from circle grid analysis in the principle strain space. Grids with closely spaced non-contacting circles with

2.45 mm diameter were electrochemically etched on the surface of the sheets in order to allow the principal strains to be measured following the procedure described in section 3.2. The strains at the onset of failure were obtained from the circles placed immediately adjacent to the crack. The experiments were done in random order and several replicates were produced for each test case in order to provide statistical meaning.

The geometric accuracy of the sheet metal parts was analysed by comparing its deviations to the specified CAD drawing that was utilized for generating the tool path in a TESA micro-hite 3D coordinate measuring machine.

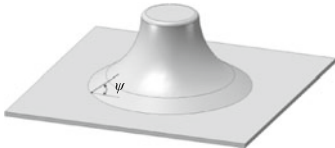
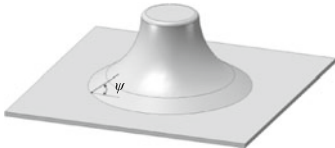
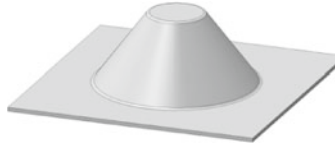
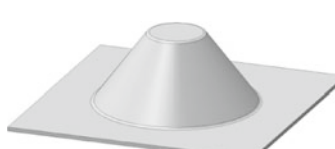
4. Results and Discussion

The first part of this section examines the mechanics of deformation of TPIF with partial die by combining circle grid analysis, material formability limits, and the unified theoretical framework proposed in section 2. The second part is focused on thickness variation and geometrical accuracy of the truncated conical parts produced by TPIF with partial die. Results from SPIF tests are included for reference and comparison purposes.

4.1 Mechanics of Deformation

The region of interest to analyse the differences in formability between SPIF and TPIF with partial die was selected by means of SPIF reference tests performed in truncated conical shapes with progressively increasing drawing angles $\psi(h)$ with the depth.

Table 3 The plan of experiments

Process	Geometry	Tool radius, mm	$\psi_0, ^\circ$
SPIF		4	30
		6	
	truncated conical shape with increasing angle with the depth		
		4	65-70
		6	61-70
TPIF partial die		4	68-76
		6	64-73
	truncated conical shape with constant angle		

The experimental distribution of the major and minor in-plane surface strains obtained from circle grid analysis that resulted from these tests is shown in Fig. 5. Results confirm that truncated conical shapes are formed under plane strain conditions and that formability decreases with the increase of the tool radius r_{tool} . The agreement between the FFL and the experimental fracture strains measured for the conical parts produced with tools having radius equal to 4 and 6 mm is very good and allowed authors to select the range of values for performing TPIF and SPIF (for comparison purposes) tests with constant drawing angles.

As seen in Fig. 6(a), the limiting drawing angles in SPIF with constant drawing angles are nearly 10° below those obtained with progressively increasing drawing angles $\psi(h)$ with the depth. This result is in close agreement with Hussain and Gao (Ref 14), which claim the maximum drawing angle ψ_{max} obtained from parts formed at fixed slopes to be smaller than that obtained from parts formed with their slopes varying with depth.

Having determined the experimental values of SPIF for comparison purposes, discussion will now be focused in the results of circle grid analysis that are plotted in the principal

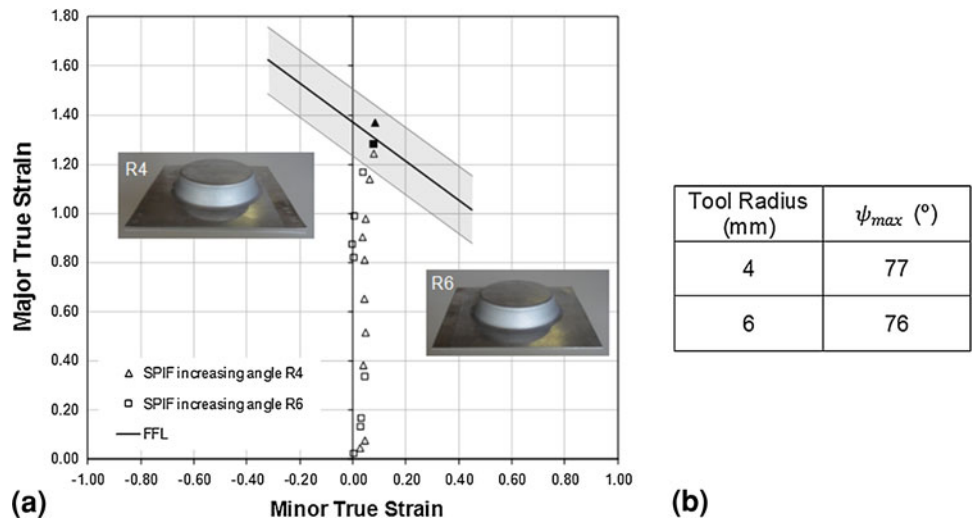


Fig. 5 (a) Experimental strains and (b) maximum drawing angles for truncated conical parts produced by SPIF with progressively increasing drawing angles $\psi(h)$ with the depth. The solid marks correspond to fracture points

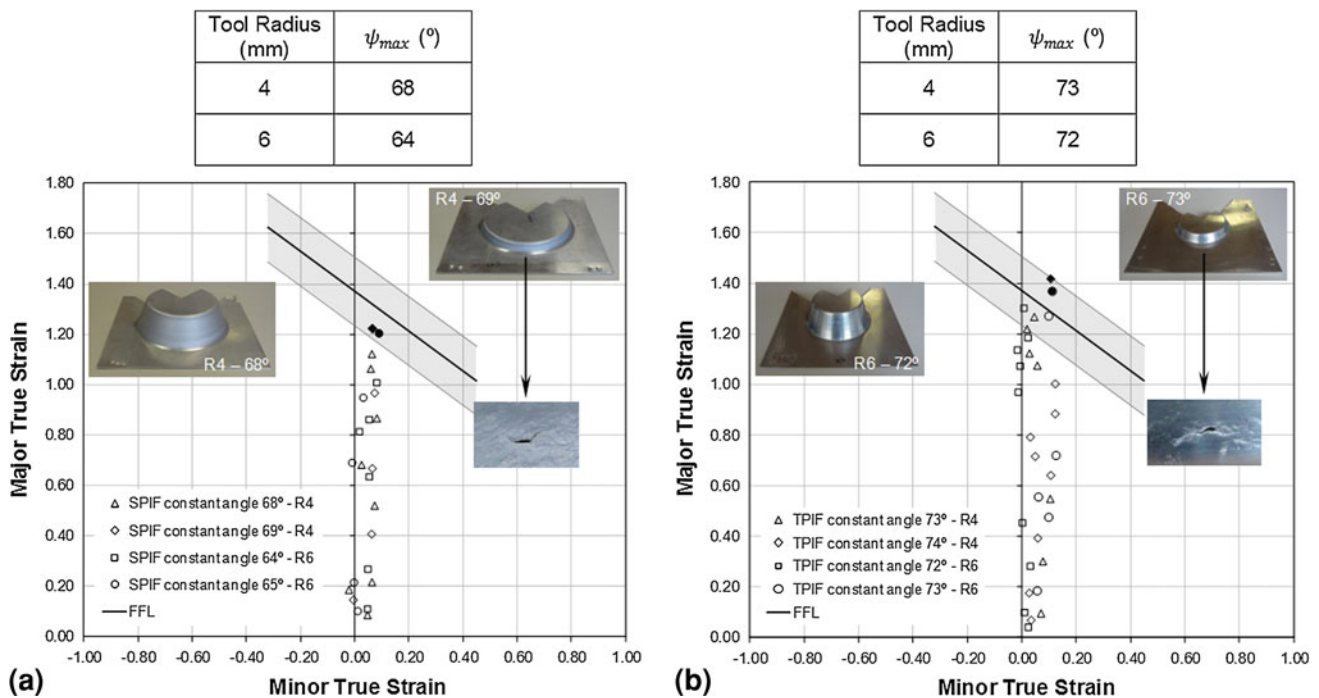


Fig. 6 Experimental strains and maximum drawing angles for truncated conical parts produced by (a) SPIF and (b) TPIF with partial die, with constant drawing angles. The solid marks correspond to fracture points

strain space for the test cases of TPIF with partial die that are listed in Table 3. The experimental observations and measurements included in the principal strain space of Fig. 6(b), highlight three main findings. Firstly, rotational symmetric parts produced by TPIF with partial die are formed under plane strain conditions. Secondly, formability limits of TPIF with partial die are higher than those of SPIF. Thirdly, the formability limits of TPIF with partial die increase when the radius of the forming tool r_{tool} decreases.

The first finding provides experimental evidence for the assumptions that were made during the development of the unified theoretical framework. The second and third findings that may also be observed in Fig. 7, are in close agreement with the theoretical estimates provided by the framework (refer to Eq 7 and Table 1) namely, in what regards the influence of operative parameters in the overall triaxiality ratio σ_m/σ_Y .

The morphology of the cracks emerging around the circumferential direction at the transition zone between the inclined wall and the bottom corner radius of the flange (refer to the inset picture in Fig. 6b) proves that deformation mechanics in TPIF with partial die is the result of in-plane stretching due to meridional tensile stresses σ_ϕ . The agreement between the FFL and the experimental fracture strains allows concluding that plastic deformation takes place by uniform thinning until fracture. In other words, there is no localized necking before reaching the onset of fracture in TPIF with partial die.

4.2 Thickness and Geometrical Accuracy

Figure 8 shows the evolution of the wall thickness along the meridional cross section of truncated conical parts produced by SPIF and TPIF with constant drawing angles $\psi(h)$ with the

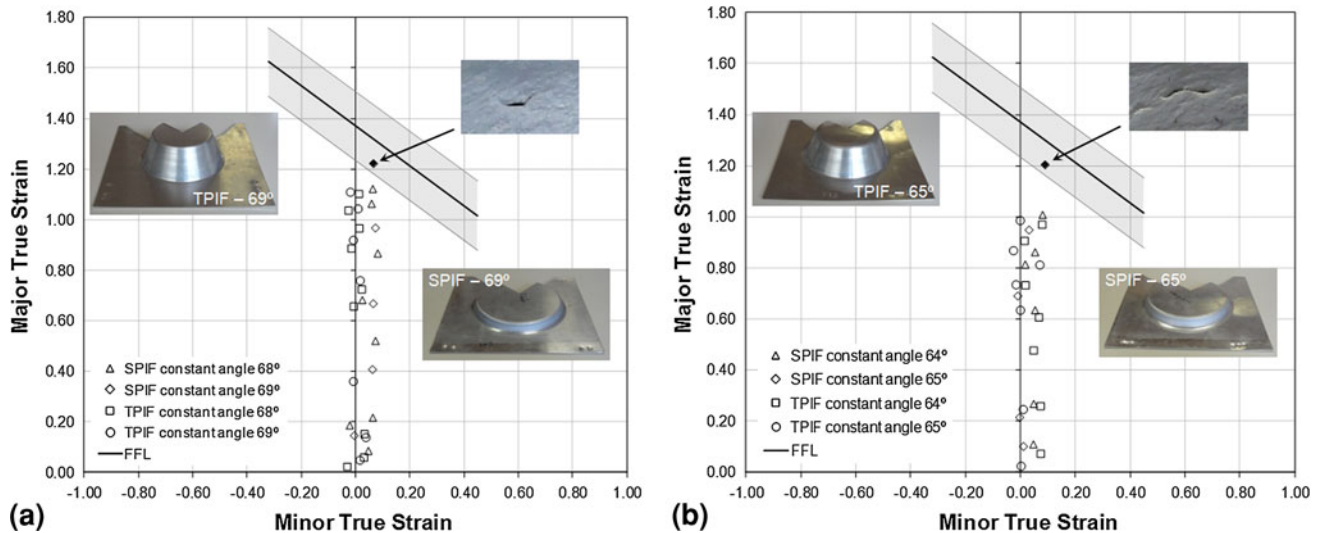


Fig. 7 Experimental strains and maximum drawing angles for truncated conical parts produced with constant drawing angles by (a) SPIF and TPIF, with a tool radius 4 mm and (b) SPIF and TPIF, with a tool radius 6 mm. The solid marks correspond to fracture points

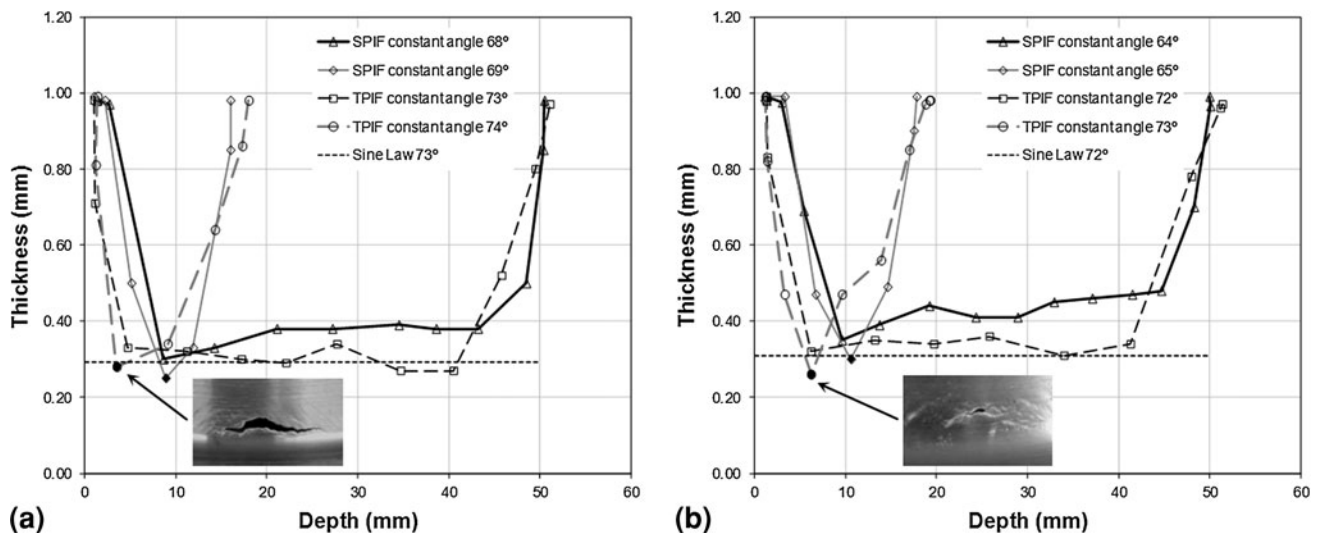
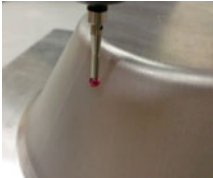


Fig. 8 Experimental evolution of thickness with depth for truncated conical parts produced by SPIF and TPIF with partial die, with constant drawing angles, with (a) tool radius of 4 mm and (b) tool radius of 6 mm. The solid marks correspond to fracture points and the dashed lines correspond to estimates provided by the sine law

Table 4 Geometrical accuracy of the experimental test parts produced by SPIF and TPIF with partial die. The enclosed detail shows the probe of the CMM machine on the surface of a test part

Process	Center deviation, mm	Angle deviation, %
SPIF	0.41	0.32
TPIF partial die	0.23	0.03



depth. As seen in Fig. 8(a) and (b) there are two completely different patterns. In case of sheet metal parts produced by SPIF and TPIF with drawing angles below the limiting drawing angle ψ_{\max} , plastic deformation takes place by uniform thinning and thickness of the inclined wall can be easily and effectively estimated by means of the sine law. This observation is in close agreement with Matsubara (Ref 4). However, results also show that failure by fracture due excessive thinning occurs for limiting drawing angles ψ_{\max} that are smaller in SPIF than in TPIF with partial die. Moreover, these values decrease as the radius of the tool r_{tool} increases.

The aforementioned experimental observations are in close agreement with the mechanics of deformation inferred from circle grid analysis and the unified theoretical framework and explain the differences in formability between SPIF and TPIF with partial die.

The geometrical accuracy of SPIF and TPIF with partial die was evaluated by comparing deviations between the specified CAD geometry, which was utilized for generating the tool path strategy, and that resulting from experimental measurements in the incrementally formed parts. The deviations between the centers and the angles of the circles of the truncated conical parts listed in Table 4 show that the overall accuracy of TPIF parts is higher than that of SPIF parts.

In practical terms the aforementioned results prove that springback will rise whenever a sheet metal part currently produced by TPIF with partial die is to be fabricated by SPIF. A possible explanation for the smaller elastic recovery of TPIF is the tensile meridional stresses $\sigma_{\phi}^{\text{bh}}$ due to external loading applied by the blank holder during its vertical movement. In fact, contrary to SPIF where the relevant stress field is local and exclusively due to progression of deformation by the moving tool, the external loading applied by the blank holder in TPIF superimposes a uniform distribution of tensile meridional stresses throughout the sheet that is capable of reducing the amount of springback that is due to the loss of contact between the tool and the local region of the sheet placed in contact with the moving tool.

5. Conclusions

The proposed theoretical framework for rotational symmetric single (SPIF) and two-point (TPIF) incremental forming is capable of successfully addressing the influence of the major operating parameters and explaining the differences in formability between the two processes.

Plots of the experimental results from circle grid analysis in the principal strain space and observations of crack opening

along the circumferential direction at the transition region between the inclined wall and the corner radius of the parts reveals that fracture in TPIF with partial die is not preceded by localized necking and that crack propagates under tensile meridional stresses acting in stretching modes of deformation.

Experimental strain loading paths validate the claim of plane strain deformation that was assumed in the proposed theoretical framework and confirm that FLCs that give the maximum strains the material can undergo before necking are not relevant to the formability limits in TPIF with partial die. It is the fracture FFL that must be employed.

The investigation also reveals that geometric accuracy of incrementally formed parts produced by TPIF with partial die is better than that of parts fabricated by SPIF due to smaller elastic recovery upon unloading.

Acknowledgments

The work of MSc. Tiago Martinho and MSc. Valter Robalo during the research work is greatly acknowledged.

References

1. J. Jeswiet, F. Micari, G. Hirt, A. Bramley, J. Dufloy, and J. Allwood, Asymmetric Single Point Incremental Forming of Sheet Metal, *Ann. CIRP*, 2005, **54**, p 623–650
2. K. Jackson and J. Allwood, The Mechanics of Incremental Sheet Forming, *J. Mater. Process. Technol.*, 2009, **209**, p 1158–1174
3. P.A.F. Martins, N. Bay, M. Skjoedt, and M.B. Silva, Theory of single point incremental forming, *Ann. CIRP*, 2008, **57**, p 247–252
4. S. Matsubara, A Computer Numerically Controlled Dieless Incremental Forming of a Sheet Metal, *J. Eng. Manuf.*, 2001, **215**, p 959–966
5. A. Attanasio, E. Ceretti, C. Giardini, and L. Mazzone, Asymmetric Two Points Incremental Forming: Improving Surface Quality and Geometric Accuracy by Tool Path Optimization, *J. Mater. Process. Technol.*, 2008, **197**, p 59–67
6. J. Jeswiet, J.R. Dufloy, and A. Szekeres, Forces in Single Point and Two Point Incremental Forming, *Adv. Mater. Res.*, 2005, **6–8**, p 449–456
7. G. Hirt, J. Ames, and M. Bambach, Basic Investigation into the Characteristics of Dies and Support Tools Used in CNC-Incremental Sheet Forming, *Proceedings of the International Deep Drawing Research Group Conference*, IDDRG, Porto, Portugal, 2006, p 341–348
8. M.B. Silva, M. Skjoedt, P.A.F. Martins, and N. Bay, Revisiting the Fundamentals of Single Point Incremental Forming by Means of Membrane Analysis, *Int. J. Mach. Tools Manuf.*, 2008, **48**, p 73–83
9. A.G. Atkins, Fracture in Forming, *J. Mater. Process. Technol.*, 1996, **56**, p 609–618
10. ASTM Standard E8/E8M, 2011, Standard Test Methods for Tension Testing of Metallic Materials, ASTM International, West Conshohocken, PA, 2011. doi:10.1520/E0008_E0008M-11

11. M. Skjoedt, M.B. Silva, P.A.F. Martins, and N. Bay, Strategies and Limits in Multi-stage Single-Point Incremental Forming, *J. Strain Anal. Eng. Des.*, 2010, **45**, p 33–44
12. A.G. Atkins, Fracture Mechanics and Metal Forming: Damage Mechanics and the Local Approach of Yesterday and Today, *Fracture Research in Retrospect*, H.P. Rossmannith, Ed., A.A. Balkema, Rotterdam, 1997, p 327–350
13. M. Durante, A. Formisano, and A. Langella, Observations on the Influence of Tool-Sheet Contact Conditions on an Incremental Forming Process, *J. Mater. Eng. Perform.*, 2011, **20**, p 941–946
14. G. Hussain and L. Gao, A novel Method to Test the Thinning Limits of Sheet Metals in Negative Incremental Forming, *Int. J. Mach. Tools Manuf.*, 2007, **47**, p 419–435